

## Research Article

**Cite this article:** Schultz KA *et al* (2019). Study of pure and mixed clustered noble gas puffs irradiated with a high intensity ( $7 \times 10^{19}$  W/cm<sup>2</sup>) sub-ps laser beam and achievement of a strong X-ray flash in a laser-generated debris-free X-ray source. *Laser and Particle Beams* **37**, 276–287. <https://doi.org/10.1017/S0263034619000521>

Received: 31 May 2019

Revised: 24 June 2019

Accepted: 25 June 2019

First published online: 22 July 2019




**Key words:**

Clusters; electron beam emission; gas puff; laser plasma; X-ray emission

**Author for correspondence:**

K. A. Schultz, Los Alamos National Laboratory, Los Alamos, NM 87545, USA.  
E-mail: [kimberlys@lanl.gov](mailto:kimberlys@lanl.gov)

# Study of pure and mixed clustered noble gas puffs irradiated with a high intensity ( $7 \times 10^{19}$ W/cm<sup>2</sup>) sub-ps laser beam and achievement of a strong X-ray flash in a laser-generated debris-free X-ray source

K. A. Schultz<sup>1</sup> , V. L. Kantsyrev<sup>1</sup>, A. S. Safronova<sup>1</sup>, V. V. Shlyaptseva<sup>1</sup>, E. E. Petkov<sup>1</sup> , I. K. Shrestha<sup>1</sup>, M. C. Cooper<sup>1</sup>, G. M. Petrov<sup>2</sup>, A. Stafford<sup>1</sup>, C. J. Butcher<sup>1</sup>, G. E. Kemp<sup>3</sup>, J. Park<sup>3</sup>  and K. B. Fournier<sup>3</sup>

<sup>1</sup>Physics Department, University of Nevada, Reno, Reno, Nevada 89557, USA; <sup>2</sup>Plasma Physics Division, US Naval Research Laboratory, Washington, DC 20375, USA and <sup>3</sup>Lawrence Livermore National Laboratory, Livermore, California 94550, USA

**Abstract**

We present a broad study of linear, clustered, noble gas puffs irradiated with the frequency doubled (527 nm) Titan laser at Lawrence Livermore National Laboratory. Pure Ar, Kr, and Xe clustered gas puffs, as well as two mixed-gas puffs consisting of KrAr and XeKrAr gases, make up the targets. Characterization experiments to determine gas-puff density show that varying the experimental parameter gas-delay timing (the delay between gas puff initialization and laser-gas-puff interaction) provides a simple control over the gas-puff density. X-ray emission ( $>1.4$  keV) is studied as a function of gas composition, density, and delay timing. Xe gas puffs produce the strongest peak radiation in the several keV spectral region. The emitted radiation was found to be anisotropic, with smaller X-ray flux observed in the direction perpendicular to both laser beam propagation and polarization directions. The degree of anisotropy is independent of gas target type but increases with photon energy. X-ray spectroscopic measurements estimate plasma parameters and highlight their difference with previous studies. Electron beams with energy in excess of 72 keV are present in the noble gas-puff plasmas and results indicate that Ar plays a key role in their production. A drastic increase in harder X-ray emissions (X-ray flash effect) and multi-MeV electron-beam generation from Xe gas-puff plasma occurred when the laser beam was focused on the front edge of the linear gas puff.

**Introduction**

Cluster formation in supersonic gas jets provides the advantages of a gaseous target in tandem with near solid ( $\sim 10^{22}$  cm<sup>-3</sup>) intracluster atomic density (Hagena 1972; Kugland *et al.*, 2008). Laser radiation can propagate through the gas puff while being efficiently absorbed by atoms in the clusters (Petrov *et al.*, 2005). Clustered gas puffs have been studied as an alternative to solid targets for laser-plasma studies due to their inherent lack of debris. Importantly, short-pulse laser beam interaction with gas-puff plasmas can produce short X-rays bursts (1–20 keV), suitable for many applications. It has been demonstrated in the past that when X rays with energy 1–10 keV are emitted when a sub-picosecond or femtosecond laser irradiates clustered Ar (Chen *et al.*, 2007; Faenov *et al.*, 2011), Kr (Kugland *et al.*, 2008; Hayashi *et al.*, 2010; Zhang *et al.*, 2011), Xe (Ditmire *et al.*, 1997, 1998; Honda *et al.*, 2000) or mixtures like Kr-Ar (Kantsyrev *et al.*, 2016c; Zhvaniya *et al.*, 2017) or Xe-Kr-Ar (Schultz *et al.*, 2016; Kantsyrev *et al.*, 2016a). These gas puffs have also been studied for hot-electron production (Malka *et al.*, 2001; Namba *et al.*, 2006; Jha and Krishnamurthy, 2008), high-harmonic generation (Shim *et al.*, 2007; Sharma and Vatsa, 2009), and laser self-focusing (Schroeder *et al.*, 1998; Balakin *et al.*, 2016) in addition to soft and hard X-ray generation (Ditmire *et al.*, 1996; Wachulak *et al.*, 2014; Kantsyrev *et al.*, 2016c).

With the advent of chirped pulse amplification, high laser intensities of  $>10^{18}$  W/cm<sup>2</sup> can be achieved, bringing laser beam physics into the strong-field regime. Ionization within a cluster is dominated by electrons tunneling through their binding potential, which is lowered by the strong field of the laser beam and the close proximity of neighboring atoms in the cluster (Fennel *et al.*, 2010). The liberated (unbound) electrons reside inside the cluster, where frequent collisions further ionize and heat the intra-cluster plasma. These collisions can induce inner-shell vacancies in gas atoms, leading to *K*-shell emission in lower-*Z* atoms like Ar.

In this paper, we study the effects of mixing noble gases on X-ray radiation and electron-beam parameters using the Lawrence Livermore National Laboratory's (LLNL) Titan laser at the Jupiter Laser Facility. Cluster-formation efficiency and ionization are known to increase (Abraham *et al.*, 1981; Last *et al.*, 1997; Kantsyrev *et al.*, 2016a; 2016c; Zhvaniya *et al.*, 2017) with the addition of a lighter carrier gas (Ar) to heavier, more easily ionized atoms (Kr and Xe). Knowledge of gas-puff parameters such as average density and cluster size is required to understand what physical properties drive stronger X-ray emission and control the X-ray spectrum. To our knowledge, no studies have been done that simultaneously measure electron beams, laser coupling, X-ray emission in different directions, X-ray spectra, and X-ray pinhole images on two high-intensity laser platforms, as well as to perform characterization experiments on five different gas target types.

In the following, the section "Experimental details" describes the details of the experiments, while the section "Results and discussion" provides results and discussion. First, the characterization of gas-puff parameters prior to laser heating is presented. Next, X-ray (>1.4 keV) emission and conversion efficiency, measurement of the transmission of the laser pulse through the gas puff plasma, and the anisotropy of X-ray emission are described. X-ray spectroscopic observations are also included. The discussion proceeds with measurements of >70 keV electron beams. Finally, we investigate the sensitivity of X-ray flash and a multi-MeV electron beam generation in Xe to focal position inside the gas puff. The section "Conclusion" summarizes our conclusions.

## Experimental details

Five different gas puff targets were tested: Ar, Kr, Xe, and two mixed gas puffs. The two mixtures, KrAr (15% Kr – 85% Ar) and XeKrAr (13% Xe – 19% Kr – 68% Ar), were chosen based on previously reported results (Schultz *et al.*, 2016; Kantsyrev *et al.*, 2016a, 2016c). Gas ratios are in percent volume, and gas-valve backing pressure remained constant for the duration of the experiments at 600 psi (41 bar). Previous articles detail the characterization process to determine gas-puff density via Mach-Zehnder interferometry as well as estimate the size of clusters (several tens of Å) via Rayleigh scattering (Schultz, 2017).

Laser-heating experiments were performed at LLNL's Jupiter Laser Facility (JLF). The 2 $\omega$  Titan laser platform's short-pulse beam is a 527-nm, 700-fs laser pulse with up to 40 J of energy in the best focus of 10  $\mu$ m in diameter (measured at 90% of maximum intensity in focal spot), delivering an intensity of up to  $7 \times 10^{19}$  W/cm<sup>2</sup> on target. The laser pulse contrast, the ratio of peak to pre-pulse laser intensity, was as good as  $10^8$  (Kemp *et al.*, 2015). The target in these experiments was a gas puff produced by a linear, supersonic nozzle mounted to a Series 9 (Parker Co., USA) pulsed gas valve. The exit cross-section of the nozzle is rectangular (1.5  $\times$  3 mm), producing an elongated profile to study potential laser self-focusing effects (Caillaud *et al.*, 2006). The gas puffs achieve supersonic speeds and, upon cooling, produce small (a few nm diameter) clusters consisting of atoms bound by Van der Waals forces. An  $f/3$  off-axis parabolic (OAP) mirror focused the laser beam at the target 1 mm from the nozzle exit (Fig. 1). The gas-puff propagation direction was orthogonal to both the laser beam propagation direction and polarization axis.

Figure 1 shows the suite of diagnostics used in the experiments. Dynamic X-ray diagnostics included filtered, cross-

calibrated AXUV-HS5 silicon diodes (response time 1 ns) and a filtered, calibrated diamond photoconducting detector (PCD) (response time 0.7 ns). The diagnostics viewed the plasma from three directions: One vertical and two horizontal lines of sight. The horizontal packages are positioned at angle  $\theta$ , measured from the direction of laser beam incidence, and the vertical package looks directly down on the gas puff. Each package consists of three Si-diodes, filtered to record X-ray emission greater than 1.4, 3.5, and 9 keV. The vertical package also housed a PCD with a lower filter cut-off energy of 2.4 keV. Filter cut-off energy is defined by the 1/e transmission of the filter. To protect the Si-diodes and PCDs from ion and electron impacts that would skew the results, 0.5-T permanent magnets were mounted between the detectors and the plasma.

A Faraday cup detector with 12.5  $\mu$ m Cu filter, giving a (lower) cutoff energy of 72 keV, was employed for electron-beam measurements. It was located along the laser propagation direction, behind the gas puff with respect to laser beam propagation ( $\theta = 150^\circ$ ). High-energy electron spectra (0.1–19 MeV) were recorded on a shot-by-shot basis on the permanent magnet spectrometer, an electron positron proton spectrometer (EPPS) (Chen *et al.*, 2008), placed 70 cm from target chamber center (TCC). Calibrated image plate strips (BAS-SR 2040) (Maddox *et al.*, 2011) captured the spectra, which were scanned by an FLA-7000 IP scanner.

Time-integrated X-ray spectrometers and pinhole cameras were also fielded. We applied an X ray, convex crystal spectrometer with a KAP (potassium acid phthalate) crystal and spectral resolution  $\lambda/\Delta\lambda$  of  $\sim 500$ –700 (Kantsyrev *et al.*, 2016c). The two X-ray pinhole cameras (three channels each with cut-off energies 0.7, 1.4, and 3.5 keV) had a spatial resolution of 60  $\mu$ m. X-ray spectra and pinhole images were recorded on Kodak Biomax MS film. Transmission of laser energy through the gas puff was measured using a calibrated scattering plate made of Spectralon<sup>®</sup> placed 38 cm from TCC downstream from the gas puff along the laser propagation direction. A 16-bit Andor DV434 CCD camera (filtered with calibrated optical density glass filters) imaged the spatial distribution of laser light incident on the scattering plate and instituted an upper bound on laser beam absorption by the gas puff.

## Results and discussion

### Gas puff characterization

Gas-puff characterization experiments were performed independently from laser-gas-puff studies. The average density of the gas puff is measured through the use of a Mach-Zehnder interferometer, the details of which were previously published (Kantsyrev *et al.*, 2016a). As described in previous works (Schultz *et al.*, 2016; Kantsyrev *et al.*, 2016a, 2016c), a distinct advantage of our experimental setup is the ability to easily vary gas-puff atomic density by changing the gas-delay timing, which is the delay between gas-puff initialization and laser-gas-puff interaction. Figure 2 illustrates the control of gas-puff atomic density for a range of delay timings. Density measurements were taken along the 3-mm length of the puff with an estimated error of <10%. The small error is due to more accurate measurements of the width of the gas puff (Kantsyrev *et al.*, 2016a) which resulted in a better estimate of the average gas-puff density. The gas-puff densities for the reported gases have maxima between delays of 830–1000  $\mu$ s with minimum densities at 600  $\mu$ s. The details regarding the

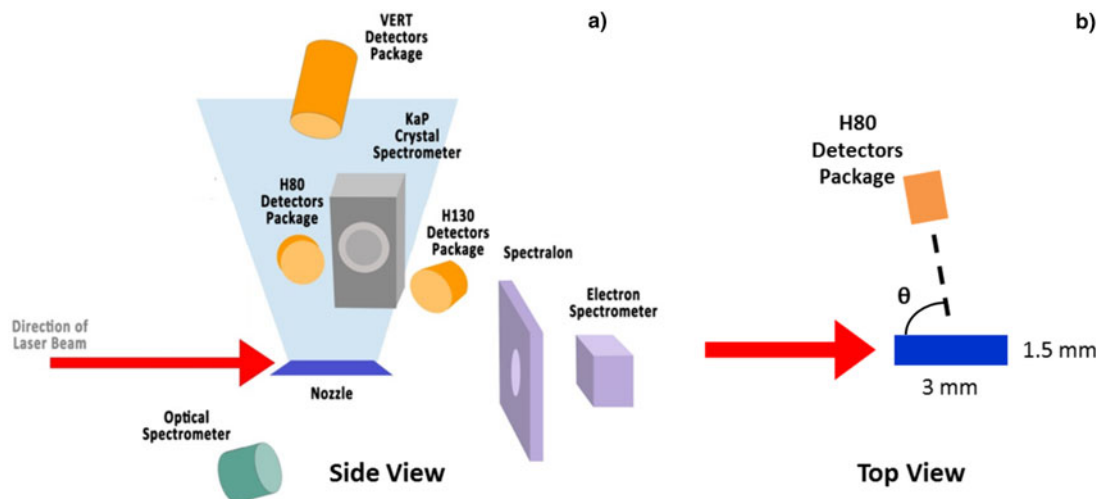


**Fig. 1.** Schematic of plasma diagnostics from (a) side and (b) top view. Laser beam polarization is into and out of the page in (a) and up and down in (b). The angle of detector packages,  $\theta$ , is measured clockwise from the direction of laser beam incidence with the laser beam coming from  $0^\circ$  and propagating towards  $180^\circ$ , see (b).

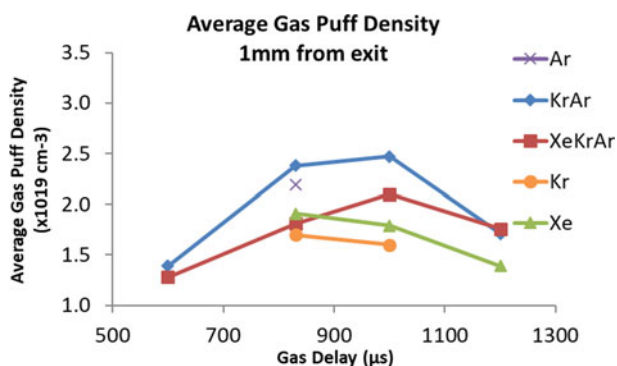


**Fig. 2.** Average particle density at the center of the gas puff 1 mm from the nozzle exit. All gas-puff targets had a backing pressure of 600 psi. Estimated error of density measurements is  $<10\%$ .

control of gas-puff density are essential since the density of the gas puff directly affects the plasma parameters and consequently, X-ray and electron emission. A combination of interferometry and Rayleigh scattering techniques were used to measure the cluster sizes of the different gas puffs. Details of these measurements can be found in Schultz *et al.* (2016) and Schultz (2017). Cluster radii at 1 mm from the nozzle exit varied from 70 to 150 Å for Ar, Kr, and mixed gas puffs and were  $\approx 200$  Å for Xe.

### X-ray emission from laser-irradiated gas-puffs

Peak X-ray-emission signals measured in the H80 detector package (Fig. 1), filtered to detect photons of  $>1.4$  and  $>3.5$  keV, are presented in Figure 3. Typical X-ray emission recorded by our time-resolved detectors lasted only several ns at full width at half maximum (FWHM), which is near the response time of the Si-diodes (0.5 ns). The temporal shape of the pulses is described in Kantsyrev *et al.* (2016a) and consists of a sharp forefront ( $<1$  ps) with a trailing edge. The vertical axes of the two plots are to scale, taking into account both individual detector sensitivity and the average spectral response of the Si-diodes  $>1.4$  and  $>3.5$  keV. For example, with Xe at a gas-puff atomic

density of  $1.4 \times 10^{19} \text{ cm}^{-3}$ , the intensity on the detector at 1.4 keV is 20 times more than that at 3.5 keV. In both spectral regions, for a given gas, the X-ray emission varies weakly with gas puff density; however, a decrease in density generally corresponds to a decrease in diode signal. Among the gas-puff gases and mixtures, Xe emits the highest amount of radiation ( $>1.4$  keV) followed by Kr and then the triple mixture.

Plasmas emit radiation through bremsstrahlung, recombination, and line-emission. The strength of each depends on electron density, electron temperature, and charge state of the plasma. Previous results (Kantsyrev *et al.*, 2016a, 2016c; Gill *et al.*, 2017) have shown that KrAr and XeKrAr gas-puff plasmas have similar electron densities and temperatures to experiments at the UNR Leopard laser. Therefore, the charge state is the leading parameter governing the power loss due to radiation. In general, the power loss scales as  $Z^x$ , where  $Z$  is the charge of the ion and  $x$  is greater than one. For bremsstrahlung and recombination radiation (Griem, 2005),  $x = 2$  and, using previously measured charge states of  $\text{Ar}^{+16}$  and  $\text{Xe}^{+30}$  gives a  $3.5\times$  increase to emitted radiation for Xe. The 3.5 keV radiation is also greatest for Xe [Fig. 3(b)], but the strength of the Ar signal increases relative to the other gases in this higher-energy region. This relative growth is due to the exclusion of Kr  $L$ -shell (1.6–2 keV) and Xe  $M$ -shell (1 keV) lines with the 3.5 keV filter.

The addition of a new diagnostic gave us the ability to determine another parameter of critical importance for the laser-gas-puff interaction: The laser transmission through the gas puff and plasma. We define the (upper bound) fraction of laser energy absorbed by the gas puff as  $\alpha$  according to

$$\alpha = \frac{E_{\text{Titan}} - E_{\text{Spectralon}}}{E_{\text{Titan}}}, \quad (1)$$

where  $E_{\text{Titan}}$  is the energy of the laser pulse and  $E_{\text{Spectralon}}$  is the amount of laser energy incident on the scattering plate (approximately an  $f/1.5$  solid angle about the laser propagation axis). It should be noted that laser energy can be spectrally or diffusely scattered by the gas puff in addition to being absorbed by the plasma or cold surrounding gas. Therefore, the reported data

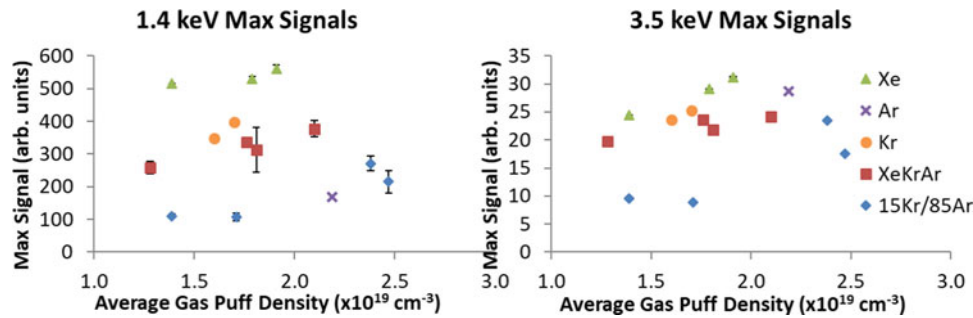


**Fig. 3.** Peak X-ray diode signals as a function of average gas puff density for two X-ray energy regions (a)  $>1.4$  keV and (b)  $>3.5$  keV. Error bars denote standard deviation on the Xe, XeKrAr, and 15Kr/85Ar data points and, in most cases, are smaller than the icons on the plot.

place an upper bound on the energy absorbed by the gas puff and plasma. We define the coefficient of conversion,  $\epsilon$ , to be a measure of how efficiently the gas puff–laser interaction converts laser energy into X rays  $>2.4$  keV. It is calculated by integrating the PCD signal in time and space ( $4\pi$  radians) and dividing by the energy of the laser pulse delivered to the gas puff. Due to anisotropy of the X-ray radiation, addressed in previous studies (Schultz *et al.*, 2016; Kantsyrev *et al.*, 2016a, 2016c) and later in this work, the values presented here provide an overestimation of  $\epsilon$ .

The relationship between  $\epsilon$  and  $\alpha$  is shown in Figure 4. Both the upper bound of energy absorption  $\alpha$  and conversion efficiency  $\epsilon$  vary with delay time (i.e. gas puff density). For all gas targets, the conversion efficiency  $\epsilon$  reaches a maximum of  $4.5 \times 10^{-4}$  at  $830 \mu\text{s}$  while the laser energy absorption approaches 100%. Absorption remains constant at  $>95\%$ , however, the conversion efficiency sharply decreases after  $830 \mu\text{s}$ . We theorize that the conversion efficiency into X rays,  $\epsilon$ , depends more strongly on the gas-puff density (and of course, plasma electron density  $n_e$ ) rather than the energy absorbed by the gas puff, due to the  $n_e^2$  dependence of the power emitted through line, recombination, and bremsstrahlung radiation rates (Griem, 2005).

In our experiments, XeKrAr consistently exhibits the lowest  $\epsilon$ , while Kr has the highest conversion efficiency. Additionally, the conversion efficiency for the double mixture is greater than that for Xe in the 2.4 keV spectral region (Fig. 4), likely due to the chosen filters ( $>2.4$  keV), which are sensitive to  $L$ -shell Kr and Ar  $K_{\alpha}$ , both of which have strong emission above the filter cut-off energy (Kantsyrev *et al.*, 2016c). The strongest  $M$ -shell Xe lines we observed in the experiments (Gill *et al.*, 2017) were emitted from 0.85 to 1.1 keV and have energies below the detection limit of the PCDs, which further helps to explain why Xe has a lower  $\epsilon$  than Kr and KrAr gas puffs. The fact that the pure gases have stronger signals is surprising considering that our previous results (Kantsyrev *et al.*, 2016a) showed that the mixtures produced the largest signals from radiation bursts. We surmise that it can be due to the different laser characteristics. The experiments in the present study were conducted at LLNL's Titan laser in its frequency-doubled mode, providing a pulse length of 700 fs at a wavelength of 527 nm, while the previous experiments (Schultz *et al.*, 2016; Kantsyrev *et al.*, 2016a, 2016c) took place at the University of Nevada, Reno's Leopard laser with 350-fs pulse length, 1.057- $\mu\text{m}$  wavelength, 15-J energy, and  $(1-2) \times 10^{19}$ -W/cm<sup>2</sup> intensity achieved with an  $f/1.5$  OAP mirror. Titan has nearly ten times the energy of Leopard and the shorter wavelength causes it to be absorbed at higher densities,

better coupling the laser beam and plasma. Not surprisingly, the absolute X-ray emission of the gas puff plasmas is larger for the Titan laser.

The most significant differences between the two systems are the laser beam wavelengths, the laser pulse durations, and the laser radiation intensity in the focal spot. The effects of pulse length on gas cluster–laser interactions at fixed laser energy have been studied (Parra *et al.*, 2001; Faure *et al.*, 2002; Kim *et al.*, 2006; Lamour *et al.*, 2007; Prigent *et al.*, 2008; Müller *et al.*, 2013). For example, in Prigent *et al.* (2008), it was determined that a longer laser pulse length decreases X-ray yield, especially with laser pulse durations in the interval of 140–800 fs. In our case, the Titan laser has a pulse that is twice as long as that of the Leopard laser, and X-ray yield (with same laser radiation intensity in the focal spot) from Titan laser would be smaller. Laser wavelength has also been shown to affect X-ray emission in clustered gas puff (Kondo *et al.*, 1997; Schroeder *et al.*, 2001; Fennel *et al.*, 2010); according to the aforementioned articles, shorter laser wavelength tends to increase X-ray yield. The radiation efficiency of clusters has been shown to have a wavelength dependence as well (Schroeder *et al.*, 1998). The  $2\omega$  Titan laser has half the wavelength of Leopard laser, and X-ray yield (with same laser radiation intensity in the focal spot) from Titan laser would be larger. The laser wavelength and pulse duration produce competing effects that compensate for each other when comparing Leopard and Titan. Therefore, the main factor will be the laser radiation intensity in the focal spot:  $7 \times 10^{19}$  W/cm<sup>2</sup> for Titan laser versus  $10^{19}$  W/cm<sup>2</sup> for Leopard laser. In our studies, X-ray generation in pure gases is increased compared to the mixed gas targets mainly due to changing dynamics of ionization and recombination processes in plasma of clustered gas puff, with an increase in the laser radiation intensity in the focal spot of approximately an order of magnitude. Examples of such phenomena are described in Faure *et al.* (2002) and Lamour *et al.* (2007) for both moderate and relativistic laser radiation intensities in the focal spot.

In these, as well as previous experiments, it was observed that the X-ray radiation is not isotropic. Strong X-ray anisotropy is observed, with the vertical Si-diodes detecting the smallest radiation signals. The degree of anisotropy was determined for the two horizontal detector packages (H80 and H130) compared to the vertical package by

$$\text{Degree of Anisotropy} = \frac{H_{\text{peak signal}} - V_{\text{peak signal}}}{H_{\text{peak signal}} + V_{\text{peak signal}}} \quad (2)$$



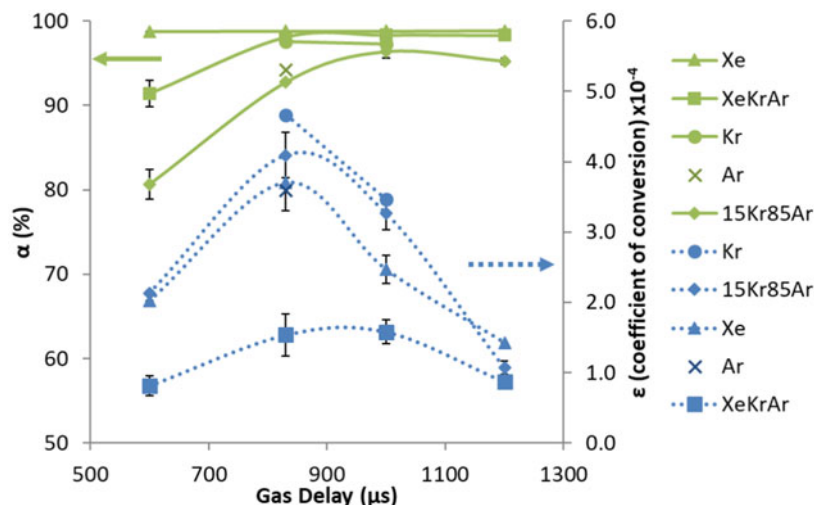


**Fig. 4.** Coefficient of conversion of laser energy into X rays,  $\epsilon$ , and fraction of absorbed laser energy by the gas puff,  $\alpha$ , as a function of gas-puff delay time. Error bars denote standard deviation.

Table 1 shows the results of the calculations averaged over the entire Titan experimental campaign including each delay time and each gas target type. They can be summarized as follows. First, the degree of anisotropy is constant regardless of gas target type. Second, it is relatively independent of the horizontal detector position with the H80 and H130 degrees of anisotropy being similar. Third, harder X-ray radiation is more anisotropic. Finally, this anisotropy is not due to laser beam polarization inducing dipole radiation from the electron cloud. We observed the same anisotropy in the experiments at the Leopard laser; the Leopard and Titan lasers have linearly polarized beams in orthogonal directions: Vertical and horizontal, respectively. If laser beam polarization were the primary cause of the anisotropy, we would have observed a change in the anisotropy that favors emission in the vertical direction for the Titan laser (perpendicular to laser beam polarization).

As discussed in the next section, several spectroscopic lines are optically thick, indicating reabsorption of photons by the plasma. This absorption causes a drop in the detected radiation but does not contribute to the observed anisotropy, assuming the colder plasma surrounding the focal spot was azimuthally symmetric about the laser propagation direction. However, because the gas puff propagation is in the vertical direction (Fig. 1), the amount of cold (<300 K), un-ionized gas between the plasma core and detectors is greatest for the vertical detectors. This provides the most plausible explanation for the anisotropy. Estimates of X-ray photon transmission through the cold gas puff above the focal spot suggests a transmission of <10% for photons with energy <4 keV. This transmission reaches 50% at ~15 keV for Kr or Xe gas; Ar is quite transparent to X rays >4 keV. However, the increased transmission of higher-energy X rays conflicts with the larger degree of anisotropy at 3.5 keV compared to 1.4 keV.

#### X-ray spectroscopy of laser-irradiated gas puffs

To provide a better understanding of the plasma conditions, X-ray spectroscopic measurements (integrated into both time and space) were performed. We are looking for a comparison of the electron temperature and density in the presented experiments with data obtained early in the UNR Leopard laser shots (Kantsyrev *et al.*, 2016a, 2016c): Will the laser-produced, gas-puff

plasmas be hotter or cooler, more dense or less? The same time-integrated, X-ray spectrometers and pinhole cameras and the same set of time-resolved X-ray detectors were used in both studies. Non-local thermodynamic equilibrium (non-LTE) kinetic modeling of the observed *L*-shell Kr and *K*-shell Ar spectra delivers estimates of the electron temperature  $T_e$  and electron density  $n_e$ , and furthermore, yields insight into the different radiative signatures from pure versus mixed gas-puff plasmas. The two non-LTE models used here have been previously employed to analyze and model *L*-shell Kr and *K*-shell Ar spectra produced from experiments on the 1 $\omega$  1.057- $\mu$ m UNR Leopard Laser (Schultz *et al.*, 2016; Kantsyrev *et al.*, 2016a, 2016c). The atomic data for both models is calculated using the Flexible Atomic Code (Gu, 2008). For the *L*-shell Kr model, the ground states are included for every ionization level, and we specify details for H-like to Al-like ions in singly and doubly excited states. In particular: The singly excited states are included up to  $n=6$  for H-like ions, with a total of 30 levels, and  $n=5$  for He-like and Li-like ions, where a total of 90 and 101 levels are included. For Be-, B-, C-, N-, O-, and F-like ions, we include up to  $n=4$  with a total of 128, 169, 401, 486, 421, and 268 levels, respectively. Up to  $n=5$  is specified for Ne-like and Na-like ions, where a total of 141 and 1029 levels are included and a total of 1273 and 385 levels up to  $n=4$  for Mg-like and Al-like ions, respectively, are included. The doubly excited states include up to  $n=3$  for He-, Li-, Na-, Mg-, and Al-like ions, and  $n=2$  for Be-like ions. Altogether, the Kr model has 4957 levels. The *K*-shell Ar model has a similar energy structure and is described with more detail in Kantsyrev *et al.* (2016c). The intensities of the synthetic spectra depend on theoretical plasma parameters such as electron temperature  $T_e$ , electron density  $n_e$ , and a fraction of hot electrons  $f$ , if present.

Examples of two experimental spectra collected using the KAP crystal spectrometer described in the section “Experimental details,” along with corresponding modeling, are shown in Figures 5 and 6. Specifically, Figure 5 shows the results from Titan shot #23 using pure Kr, and Figure 6 displays results from Titan shot #11 using the KrAr mixture. The raw experimental data are at the top of each figure. In order to model the spectra, a lineout is first taken across each film, and the corresponding intensities are adjusted for the 2- $\mu$ m doubly aluminized Mylar filter placed between the radiation source and KAP crystal in the

**Table 1.** Degree of anisotropy of X-ray emissions in two spectral regions for two horizontal detector positions

Detector package (Spectral region)	Average degree of anisotropy
H80 (1.4 keV)	$0.26 \pm 0.06$
H130 (1.4 keV)	$0.24 \pm 0.07$
H80 (3.5 keV)	$0.64 \pm 0.10$
H130 (3.5 keV)	$0.72 \pm 0.18$

Results are averaged over the entire experimental campaign.

spectrometer. Additional pre-processing includes calibrating the raw spectra to the appropriate wavelength region. Finally, the experimental plasma parameters are estimated by matching theoretical line intensities to the experimental ones.

Spectroscopic modeling for Titan shot #23 with pure Kr indicates an electron temperature of  $T_e = 640$  eV and an electron density of  $n_e = 5 \times 10^{18} \text{ cm}^{-3}$ . The uncertainty in the determination of an electron temperature  $T_e$  was  $\pm 10\%$ , and an electron density  $n_e$  was  $\pm 10\%$ . The electron density is estimated by matching the intensity of the Ne-like 3F and 3G lines. The electron temperature instead uses the intensity ratio of the Na-like satellite lines near the Ne-like 3C and 3D lines, as well as matching the intensity of the mostly optically thin 2–4 transitions which are on the lower end of the wavelength region in the spectrum. The estimated electron density is an order of magnitude lower than the atomic density and, with Ne-like Kr evident in the spectra, one would expect electron densities on the order of  $10^{21} \text{ cm}^{-3}$ . However, previous MD modeling (Kantsyrev *et al.*, 2016a) suggests nearly instantaneous (several fs) disassociation and explosion of the gas clusters. Pinhole camera images (Fig. 12) also demonstrate that the plasma has expanded significantly, evidenced by the smaller emission region at higher X-ray energies. This explains the lower densities from the spectral fit. We conclude that the spectral lines presented in Figures 5 and 6 at 3.7–8 Å (3.4–1.5 keV) are generated in the hot central region of the plasma.

For Titan shot #11 with the KrAr mixture, the spectrometer recorded both *L*-shell Kr and *K*-shell Ar radiation. Non-LTE modeling of these signatures indicates an electron temperature of  $T_e = 580$  eV and an electron density of  $n_e = 4 \times 10^{18} \text{ cm}^{-3}$  for *L*-shell Kr, and  $T_e = 650$  eV and  $n_e = 5 \times 10^{19} \text{ cm}^{-3}$  for *K*-shell Ar. The plasma in Titan shot #23 is almost optically thin, evidenced by comparing the ratios of the 3C and 3D line intensities and the shape of the lines. We are also able to describe the 2–4 transitions that are usually much less influenced by opacity effects. For Titan shot #11 however, the lines appear to be broadened and optically thick. Moreover, the 3C intensity is less than 3D, which further suggests that the plasma is optically thick.

We observe that in comparison with pure Kr and KrAr gas puffs at the  $1\omega$  Leopard laser (Kantsyrev *et al.*, 2016a, 2016c), the new  $2\omega$  Titan results indicate a  $T_e$  approximately  $1.5\times$  higher and a  $n_e$  almost two orders of magnitude lower. Unlike the gas-mixture experiments on the  $1\omega$  Leopard laser, where Ar spectra showed only the “cold”  $K_\alpha$  line, the Ar spectra produced by the Titan laser manifest ionic-emission lines, namely the Ar He- $\alpha$  and intercombination (IC) lines, which are associated with much hotter *K*-shell Ar plasmas. Previously, the presence of the “cold”  $K_\alpha$  line indicated poor heating in the plasmas and we concluded that the Ar gas inefficiently clustered in the mixtures,

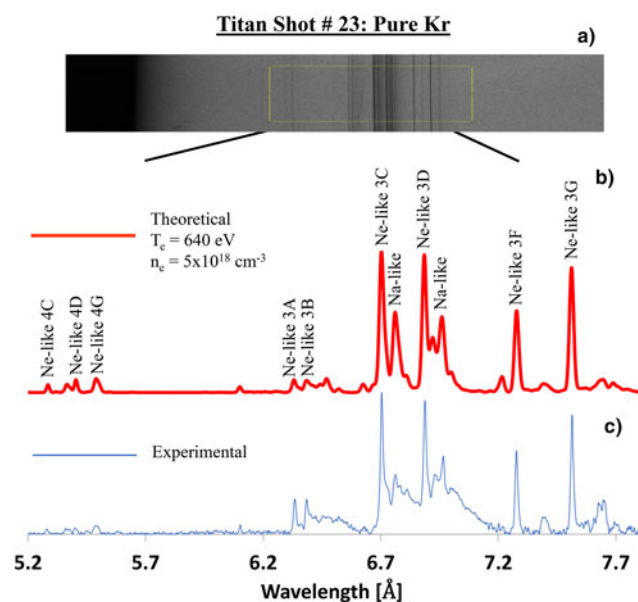


**Fig. 5.** (a) Raw, experimental *L*-shell Kr X-ray spectra produced in a pure Kr gas puff (shot #23) and captured by the KAP crystal spectrometer. The (b) red and (c) blue traces correspond to theoretical and experimental spectra, respectively.

supported by a study which showed homogeneous or heterogeneous clusters can be formed in KrAr gas-puff mixtures (Danylchenko *et al.*, 2015). However, in experiments on the Titan laser, the Ar ions in the mixture plasma produced higher-energy, ionic-emission spectra. The gas-puff properties remained constant between experiments, while the intensity in the focal spot was seven times higher with Titan than with the Leopard laser; this new data imply that Ar does in fact cluster in the mixtures, but requires more incident laser power to produce ionic-emission lines. Hence, a change in laser beam parameters drives different phenomena in the gas puffs.

#### Electron beam generation in laser-irradiated gas puffs

Faraday cup signals for electrons with energy  $>72$  keV (12.5  $\mu\text{m}$  Cu filter) were collected along the laser beam path directly behind the gas puff (Fig. 1) and lasted 10–15 ns. Figure 7 implies that electron beam current is relatively independent of the gas delay. However, the gas type does affect the magnitude of the current. The total charge in the electron pulses was in the  $\mu\text{C}$ -range. The triple mixture exhibits the highest peak electron beam current at 0.76 kA compared to both the KrAr mixture and Ar with the smallest current at around 0.5 kA. Previous experiments (Kantsyrev *et al.*, 2016a) with gas-puffs on the Leopard laser showed a peak beam current of 0.6 kA, meaning a 20% increase in current for XeKrAr was achieved. The double mixture experienced an even larger increase. On the Leopard laser, an electron beam current of 0.2 kA was observed for KrAr, compared to 0.5 kA on Titan, which is a  $2.5\times$  increase.

The EPPS was used to record spectra of  $>100$  keV electron and proton/ion beams. Ar and KrAr gas puffs reliably produced measurable electron spectra. For the KrAr mixture, the shots with observable spectra are shown in Figure 8. The left axis is normalized by electron energy and the solid angle of detection. The time-fade of the image plate signal was also taken into account (Maddox *et al.*, 2011). Note that the electron quiver energy in

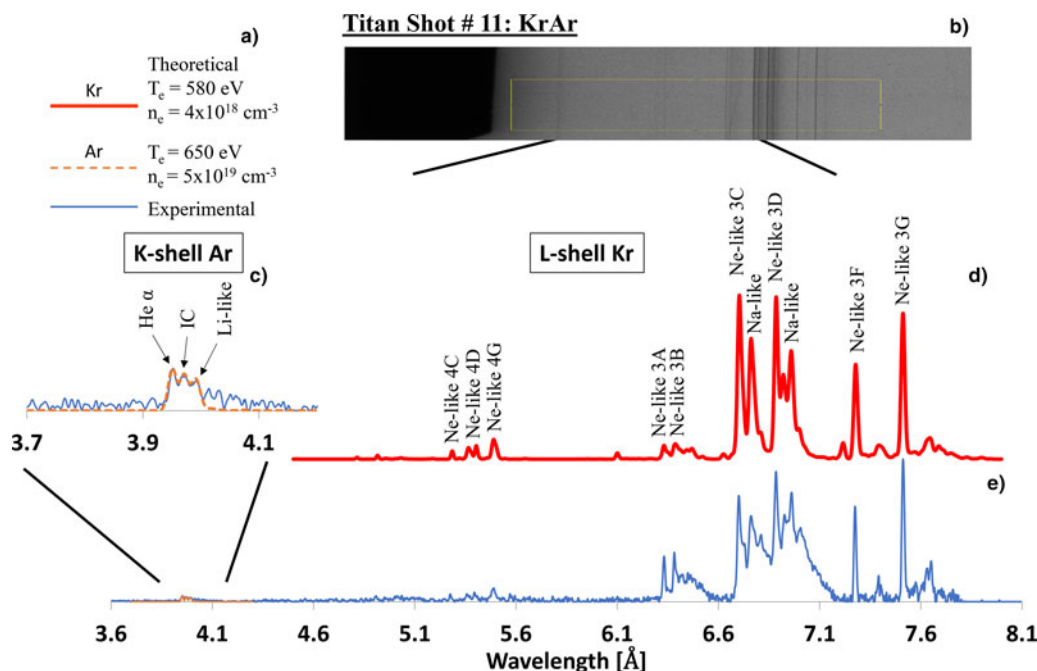


**Fig. 6.** (b) Raw, experimental X-ray spectra produced in a KrAr gas puff and captured by the KAP crystal spectrometer (shot #11). (a) The legend displays results of modeling electron temperature  $T_e$  and density  $n_e$  for Kr and for Ar, respectively. (c) the dashed (orange) trace corresponds to theoretical K-shell Ar spectra, and the solid (blue) trace correspond to experimental K-shell Ar spectra in region 3.7–4.1 Å, respectively. Also, (d) thick (red) and (e) thin (blue) traces correspond to theoretical and experimental L-shell Kr spectra, respectively.

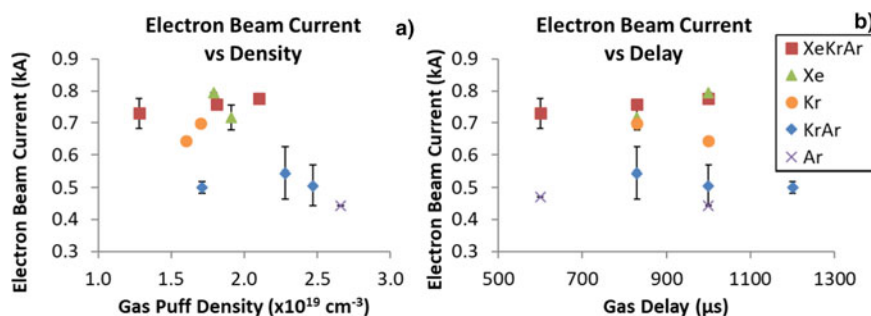


**Fig. 7.** Electron beam current as a function of gas-delay time measured by Faraday cups. Error bars represent the standard deviation of the data when multiple shots were available.

the laser field is 7 MeV and its effect is not observed in our experiments. Multiple shots were performed at each gas delay and, while the magnitude of detected electrons varies, the maximum counts occurred reliably at 0.5–0.6 MeV. For comparison, the Ar gas puffs also produced spectra peaked near 0.7 MeV. The FWHM of the spectra varied between 0.2 and 0.6 MeV, with both the 600 and 1000  $\mu$ s delay being on the lower side of the range.

Included in **Figure 8** are several exponential fits to the data using  $\gamma(E) = e^{-E/kT}$ , with  $E$  as electron energy and  $kT$  as the temperature of the electrons. These fits indicate slope temperatures of 0.4–0.6 MeV and are consistent with an effective temperature of the “hot electrons,” a fast electron component moving along the laser propagation direction, generated by sub-picosecond lasers at near-relativistic intensities. The scaling of the hot electron temperature with laser intensity and wavelength is well known (Beg *et al.*, 1997; Chen *et al.*, 2009)

$$T_{\text{hot}} \sim (I\lambda^2)^{1/3}.$$

For the frequency-doubled Titan laser, Beg’s formula (Beg *et al.*, 1997),  $T_{\text{hot}} \cong 100(I_{17}\lambda^2[\mu\text{m}])^{1/3}$ , yields  $T_{\text{hot}} \cong 580$  keV. This estimate agrees with the highest slope temperature of the electron spectra measured in our experiment (**Fig. 8**).

In contrast to the double mixture and pure Ar, no high energy electrons were detected for any pure Kr gas puff. Therefore, Ar must be a strong factor in the production of high energy (>100 keV) electrons. In mixed gas puffs, it was previously reported (Kantsyrev *et al.*, 2016a, 2016c) that Ar gas in the targets does not produce clusters, as evidenced by the presence of the cold  $K_{\alpha}$  line observed in a non-clustered gas puff. This spectroscopic line in the absence of more thermal X rays (low background noise) indicates an electron beam in the plasma strong enough to produce inner shell vacancies. The EPPS also could not detect electron spectra for Xe and XeKrAr mixture gas puffs. Out of the 11 XeKrAr shots, only one produced an analyzable electron spectrum that peaked sharply at 0.7 MeV (FWHM of 340 keV). Eleven Xe shots produced no measurable spectra. The Faraday cup data show that the Xe and triple mixture plasmas produce electrons with at least 72 keV in energy. It is

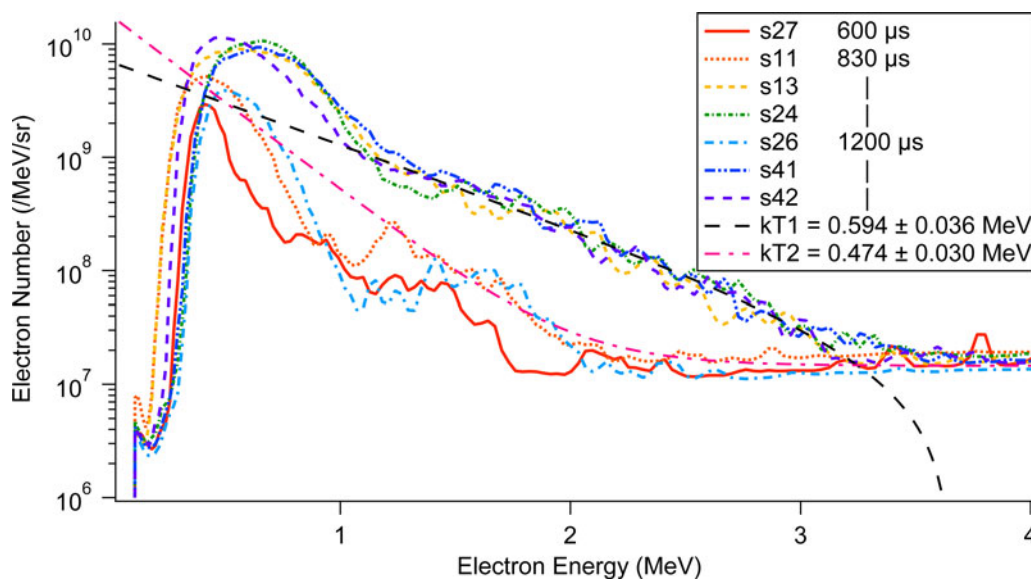


**Fig. 8.** Electron spectra recorded by the EPPS for different delays of the KrAr gas-puff targets. Exponential fits of shots 42 and 11 ( $kT_1$  and  $kT_2$ , respectively) indicate slope temperatures of 0.594 and 0.474 MeV.

surmised that the electron beam energy in the pure and mixed Xe gas puffs might not exceed the detection threshold of the spectrometers. Another reason for measurable Faraday cup signals but no detectable spectra may be due to electron beam interactions with gas-plasma-vacuum boundaries or with the plasma itself.

**Achievement of a strong X-ray flash and MeV-scale electron beams from a laser-irradiated gas puff**

During the experiments described so far, the laser beam was focused in the center of the gas puff (Fig. 1). Additional shots scanned the focal spot position of the laser beam incrementally towards the front edge of pure Xe gas puffs (at a gas delay of 830  $\mu$ s) as indicated in Figure 9. This produced drastic changes in X-ray emissions and electron-beam generation from Xe laser-irradiated gas-puff plasmas (Kantsyrev *et al.*, 2016b).

Maximum Si-diode signals for focal scan sequence of shots are summarized in Figure 10 for the detectors located at  $\theta = 130^\circ$ , though the same trends are seen in all observed directions. In the softer X-ray region ( $>1.4$  keV), the strongest signals are observed for  $y = 0$  mm and decrease with increasing parameter  $y$ . In the harder X-ray regions, both the  $>3.5$  keV and  $>9$  keV Si-diodes detected increasing X-ray emission with an increase in the  $y$  parameter (Fig. 9). Note that throughout the described experimental campaign, including the results in the previous section, signals on the 9 keV diode were weak, and only occasionally rose above noise levels. A sharp jump in the X-ray yield  $>9$  keV is observed for  $y = 1.5$  mm and saturated the signals on the oscilloscope. Even though the 9 keV signals do not show the true peak measurement, they are still presented to show the drastic difference in signal strength.

We see a six- to eightfold increase in  $\epsilon$ , in the vertical direction, upon moving the focal spot to the front edge of the gas puff with a value for  $\epsilon$  of  $2.16 \times 10^{-3}$ ; this comes with no change to the absorption of the gas puff, meaning that another process must contribute to the increase in X-ray efficiency.

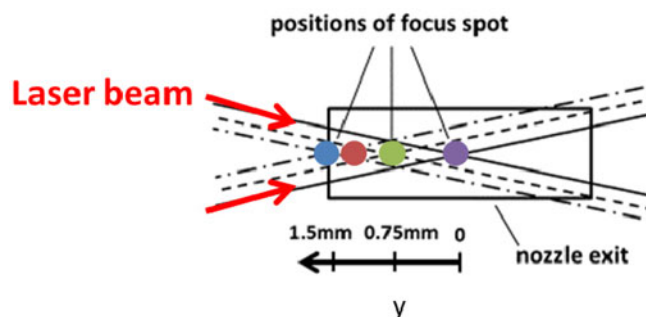


**Fig. 9.** Location of the four shots taken at various values of  $y$  overlaid on the supersonic linear nozzle exit. View from the top.

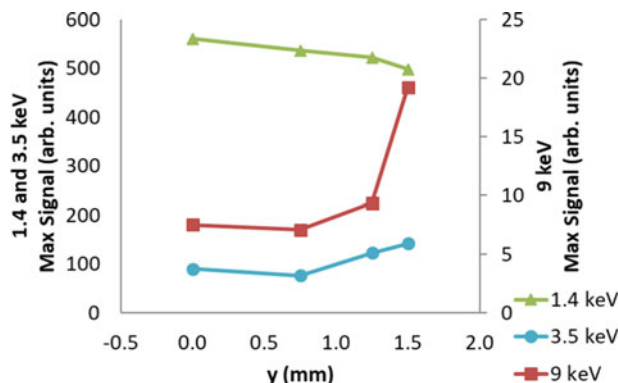


**Fig. 10.** Relative intensity of Xe gas-puff plasma X-ray emissions for the scanned laser focal spot positions measured by Si-diodes at 1.4, 3.5, and 9 keV.

Titan-irradiated 10- $\mu$ m-thick Ag and Mo foils served as a comparison for our laser-irradiated gas puffs. Most impressively, the magnified  $\epsilon$  at  $y = 1.5$  mm is only 1.5 times smaller for the gas puffs compared to the Ag or Mo foil targets. Additionally, films



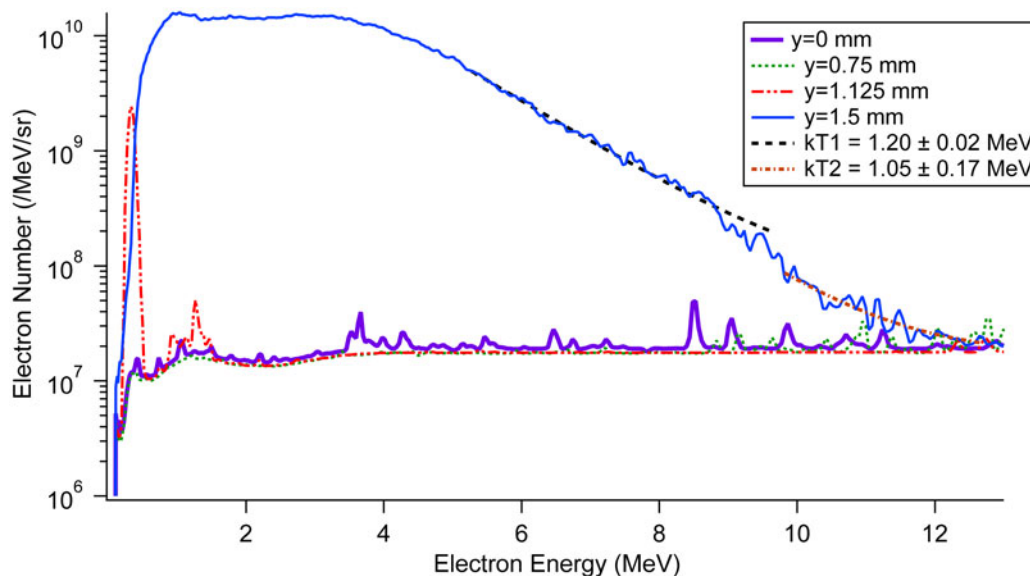


**Fig. 11.** Xe focal scan electron spectra measured by the EPPS. The  $y = 0$  and 0.75-mm shots demonstrate the lack of measurable spectra for the other Xe gas puffs. The two  $kT$  lines are exponential fits of the  $y = 1.5$  mm spectra indicating temperatures of 1.20 and 1.05 MeV.

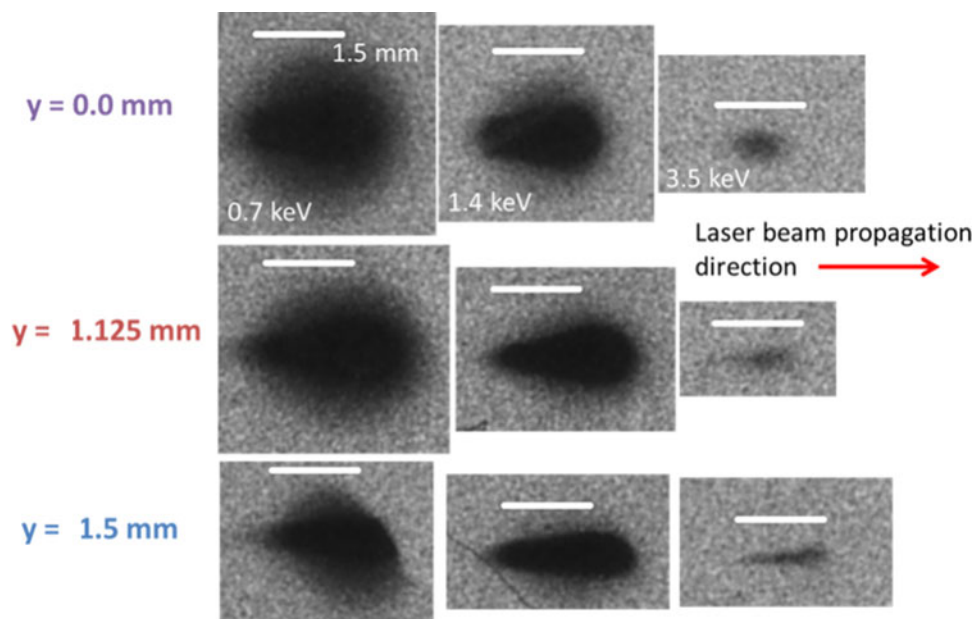


**Fig. 12.** Xe focal scan pinhole images in the 0.7, 1.4, and 3.5 keV spectral regions (left to right). The gas puff propagates out of the page and the white bar in each image represents 1.5 mm.

**Table 2.** Full length at half maximum along the laser beam propagation direction of the X-ray emitting regions at 3.5 keV from Figure 12 for different focal spot locations

Y (mm)	0	0.75	1.125	1.5
FWHM (mm)	0.77	0.29	1.39	1.2

in both X-ray spectrometers partially blackened during the front-focus shot, indicating the production of X rays with energies in the several tens of keV. In fact, the  $1/e$  cut-off energy of the shielding on the spectrometer's X-ray film was 175 keV. This regime of

X-ray generation from clustered Xe gas puffs irradiated by sub-ps laser pulse is termed an “X-ray flash”. Another profound difference occurred in both low and high energy electron emissions. Peak electron current during the Titan campaign hovered around 0.4–0.7 kA for all gas targets. However, laser-irradiated Xe gas puffs at  $y = 1.125$  mm reached a peak current of 1.52 kA, more than doubling the current of previous shots.

EPPS data for the four focal scan positions, shown in Figure 11, further highlights the regime change. The only  $y$ -values with measurable spectra are 1.125 and 1.5 mm. In complete contrast to the narrow energy bandwidth of the other laser-irradiated gas puffs (Fig. 8), a broad, strong spectrum arose for  $y = 1.5$  mm.

The FWHM of the electron spectrum at  $y = 1.5$  mm is 4 MeV, an order of magnitude larger than those reported earlier in this work, with the range of the flattop (at  $\sim 14 \times 10^9$  /MeV/sr) being 0.94–3.30 MeV. The tail of the spectrum shows good agreement with two exponential fits using temperatures of 1.2 and 1.05 MeV.

The extreme changes described in the preceding paragraphs are surmised to have resulted from the self-focusing of the laser beam at larger values of  $y$ . Figure 12 shows support for this idea found in X-ray pinhole images for several focal spot locations. The three-channel pinhole camera was located at  $\theta = 40^\circ$  (Fig. 1). The emitting region of the laser plasma exhibits a lack of definition in the lowest energy region (0.7 keV). However, as the filter cut-off energy increases, the X-ray emitting regions decrease in size and have sharper edges. Starting at 1.4 keV, we begin to see evidence of self-focusing in the plasma through the lengthening of the X-ray emitting region along the laser propagation direction; this lengthening is countered by apparent defocusing of the laser. On the downstream side of the images (right side) in Figure 12, the width (on the film) of the emitting region is larger, suggesting defocusing of the laser beam in the plasma.

The clearest picture in support of some self-focusing is given at 3.5 keV. The width of the X-ray emitting region has decreased compared to  $y = 0$  mm and the length has increased, which is consistent with self-focusing effects. Table 2 summarizes the FWHM of the length of the emitting region during the focal scan experiments; the angular position of the pinhole camera was taken into account in the lengths of the emitting region. A fivefold increase, compared to  $y = 0$  mm, occurs at  $y = 1.125$  mm and  $y = 1.5$  mm saw a four-fold increase. The Rayleigh length of the frequency-doubled Titan laser when focused to a spot size of  $\sim 10$   $\mu\text{m}$  is 150  $\mu\text{m}$ . Therefore, we do see evidence of self-focusing at  $y > 1.125$  mm where the X-ray emitting region at least doubles the confocal distance ( $2z_R$ ). The hypothesis of laser beam self-focusing in the gas-puff plasmas is consistent with the generation of hard X rays and accelerated MeV electrons (Alexeev *et al.*, 2003; Caillaud *et al.*, 2006; Kim *et al.*, 2006; Chou *et al.*, 2007). Density gradients on the edges of the gas puff provide the index of refraction variations necessary for relativistic and ponderomotive self-focusing of the laser beam.

## Conclusion

In conclusion, pure and mixed supersonic gas puffs were investigated as a controllable X-ray source using the 2 $\omega$  LLNL Titan laser and were compared to previous experiments with the 1 $\omega$  UNR Leopard Laser. Gas-puff characterization experiments determined the average density for the tested gases as a function of gas delay timing, an independent experimental variable. Five gases were tested: Ar, Kr, Xe, a mixture of Kr and Ar, and a triple mixture of Ar, Kr, and Xe. The pure Xe gas puffs produced the strongest radiation in each of the observed spectral regions ( $>1.4$ ,  $>3.5$ , and  $>9$  keV) for the gas-puff targets. Laser beam absorption and gas-puff material both contribute to the efficiency of converting laser energy to  $>2.4$  keV X-ray photons. This is a possible way to optimize X-ray yield; for example, the gas delay time of 830 ms produced the maximum  $\epsilon$  for most gases used in the experiments.

X-ray emissions were also found to be anisotropic, emitting less radiation in the direction parallel to gas-puff propagation and with a higher degree of anisotropy for more energetic photons. Surprisingly, the anisotropy had only small variations between gas target types and was constant over the duration of

the experimental campaign. Laser beam polarization was ruled out as it changed orientation between experimental campaigns at the Leopard (Schultz *et al.*, 2016; Kantsyrev *et al.*, 2016c) and Titan (this work) lasers and the anisotropy persisted. Decreased transmission of photons through the cold gas puff above the nozzle was proposed as an explanation. However, the increased transmission of higher-energy X rays conflicts with the larger degree of anisotropy at 3.5 keV compared to 1.4 keV. X-ray spectroscopic measurements at a position closer to the vertical diode position could shed light on the data in future experiments.

X-ray spectroscopic data further illuminated our findings. The new 2 $\omega$  Titan results indicate a  $T_e$  approximately 1.5 times higher and an  $n_e$  almost two orders of magnitude lower than previous results at the 1 $\omega$  Leopard Laser (Kantsyrev *et al.*, 2016c). Moreover, unlike the gas-mixture experiments on the 1 $\omega$  Leopard laser, where Ar spectra showed only the “cold”  $K_\alpha$  line, which indicated that the Ar gas clustered inefficiently, the Ar plasmas produced in Titan experiments manifest ionic lines, which are associated with much hotter  $K$ -shell Ar plasmas. Similarly, for the KrAr gas puffs, the Ar  $K_\alpha$  and Kr  $L_\alpha$  “cold” characteristic lines were not detected.

X-ray pinhole camera images also demonstrate that the plasma has expanded significantly after clusters dissociation, evidenced by the smaller emission region at higher X-ray energies. We conclude that observed X-ray spectral lines in region  $\sim 3.7$ – $8$   $\text{\AA}$  (3.4–1.5 keV) are generated in the hot central region of the laser plasma.

The relatively less energetic electron beams (from several keV to tens of keV), responsible for excitation of Ar  $K_\alpha$  and Kr  $L_\alpha$  “cold” characteristic lines, were not generated or were weak in the Titan-produced plasmas. At the same time, relatively strong, highly energetic non-Maxwellian electron beams with energy from several hundred keV to 1 MeV were observed with the EPPS. These high-energy non-Maxwellian electron beams were responsible for the observed bremsstrahlung radiation ( $>$ several hundred keV).

The laser-produced gas-puff plasmas generated high-energy electrons ( $>1$  MeV) and low-energy electron beams ( $>72$  keV). Electron beam current increased more than expected when generated at a laser wavelength of 527 nm and intensity of  $7 \times 10^{19}$  W/cm<sup>2</sup> (Titan laser) compared to previous results with a 1057-nm,  $10^{19}$  W/cm<sup>2</sup>-intensity laser pulse (Leopard laser). Gas-puff density also had a strong effect on electron beam current for the pure gas puffs. High-energy electrons were observed reliably on an electron spectrometer for gas puffs containing Ar, but not Xe, with peak energies up to 0.7 MeV.

Interestingly, scanning the focal-spot position towards the front edge of a linear Xe gas puff produced a strong X-ray-flash effect in harder spectral regions and generated a multi-MeV electron beam, coincident with the observation of self-focusing of the laser beam within the plasma. Evidence of X-ray emission with energy  $>150$  keV was observed and electrons with energies  $>6$  MeV were also produced in the Xe gas-puff plasma. More importantly, the maximum X-ray yield from the Xe gas puff, a debris-free source of radiation, is only 1.5 times smaller than that from Mo or Ag solid-foil targets.

Much remains to be understood about the dynamics of the plasma directly after cluster dissociation. MD modeling can estimate charge states of the plasma, but the actual expansion of the clusters and subsequent plasma is beyond the scope of this work. Future work would include a deeper study into the electron beam–plasma interactions and heating.

**Acknowledgements.** The authors would like to thank J. Moschella of UNR for his contributions to previous work as well as H. Chen of LLNL for the use of the EPPS. Additional thanks are given to the entire staff at the Jupiter Laser Facility at Lawrence Livermore National Laboratory. This work was supported by the Defense Threat Reduction Agency, Basic Research Award # HDTRA1-13-1-0033, to University of Nevada, Reno, and in part by NNSA under DOE grant DE-NA0003877. Work at LLNL was performed under the auspices of the U.S. DOE by LLNL under contract DE-AC52-07NA27344. G. Petrov was supported by the Air Force Office of Scientific Research under award number FA9550-14-1-0282.

## References

- Abraham O, Kim S and Stein G (1981) Homogeneous nucleation of sulfur hexafluoride clusters in Laval nozzle molecular beams. *The Journal of Chemical Physics* **75**, 402.
- Alexeev I, Antonsen T, Kim K and Milchberg H (2003) Self-focusing of intense laser pulses in a clustered gas. *Physical Review Letters* **90**, 103402.
- Balakin AV, Borodin AV, Dzhdzhoev MS, Gorgienko VM, Esaulkov MN, Zhvaniya IA, Kuzechkin NA, Ozheredov IA, Sidorov AY, Solyankin PM and Shkurinov AP (2016) Terahertz emission during interaction of ultrashort laser pulses with gas cluster beam. *Journal of Physics: Conference Series* **735**, 12021.
- Beg FN, Bell AR, Dangor AE, Danson CN, Fews AP, Glinsky ME, Hammel BA, Lee P, Norreys PA and Tatarakis M (1997) A study of picosecond laser–solid interactions up to  $10^{19}$  W cm<sup>-2</sup>. *Physics of Plasmas* **4**, 447–457.
- Caillaud T, Blasco F, Bontá C, Dorchie F and Mora P (2006) Study of intense femtosecond laser propagation into a dense Ar gas and cluster jet. *Physics of Plasmas* **13**, 033105.
- Chen H, Patel PK, Price DF, Young BK, Springer PT, Berry R, Booth R, Bruns C and Nelson D (2003) A compact electron spectrometer for hot electron measurement in pulsed laser solid interaction. *Review of Scientific Instruments* **74**, 1551–2076.
- Chen LM, Kando M, Ma J, Kotaki H, Fukuda Y, Hayashi Y, Daito I, Homma T, Ogura K, Mori M, Pirozhkov AS, Koga J, Daido H, Bulanov SV, Kimura T, Tajima T and Kato Y (2007) Phase-contrast x-ray imaging with intense Ar K $\alpha$  radiation from femtosecond-laser-driven gas target. *Applied Physics Letters* **90**, 211501.
- Chen H, Link AJ, van Maren R, Patel PK, Shepherd R, Wilks SC and Beiersdorfer P (2008) High performance compact magnetic spectrometers for energetic ion and electron measurement in ultraintense short pulse laser solid interactions. *Review of Scientific Instruments* **79**, 10E533.
- Chen H, Wilks SC, Kruer WL, Patel PK and Shepherd R (2009) Hot electron energy distributions from ultraintense laser solid interactions. *Physics of Plasmas* **16**, 020705.
- Chou M, Lin P, Lin C, Lin J, Wang J and Chen S (2007) Dramatic enhancement of optical-field-ionization collisional-excitation x-ray lasing by an optically-preformed plasma waveguide. *Physical Review Letters* **99**, 63904.
- Danylchenko OG, Kovalenko SI, Konotop OP and Samovarov VN (2015) Diagnostics of composition and size of clusters formed in supersonic jets of Ar–Kr gas mixtures. *Low Temperature Physics* **41**, 637–644.
- Ditmire T, Donnelly T, Rubenchik A, Falcone R and Perry M (1996) Interaction of intense laser pulses with atomic clusters. *Physical Review A* **53**, 3379–3402.
- Ditmire T, Smith RA, Marjoribanks RS, Kulcsár G and Hutchinson MHR (1997) X-ray yields from Xe clusters heated by short pulse high intensity lasers. *Applied Physics Letters* **71**, 166.
- Ditmire T, Patel PK, Smith RA, Wark JS, Rose SJ, Milathianaki D, Marjoribanks RS and Hutchinson MHR (1998) keV x-ray spectroscopy of plasmas produced by the intense picosecond irradiation of a gas of xenon clusters. *Journal of Physics B: Atomic, Molecular and Optical Physics* **31**, 2825.
- Faenov AY, Skobelev IY, Pikuz TA, Fortov VE, Boldarev AS, Gasilov VA, Chen LM, Zhang L, Yan WC, Yuan DW, Mao JY, Wang ZH, Colgan J and Abdallah J (2011) Diagnostics of the early stage of the heating of clusters by a femtosecond laser pulse from the spectra of hollow ions. *JETP Letters* **94**, 171–176.
- Faure J, Malka V, Marquès JR, David PG, Amiranoff F, Ta Phuoc K and Rousse A (2002) Effects of pulse duration on self-focusing of ultra-short lasers in underdense plasmas. *Physics of Plasmas* **9**, 756.
- Fennel T, Meiwes-Broer KH, Tiggesbäumker J, Reinhard PG, Dinh PM and Suraud E (2010) Laser-driven nonlinear cluster dynamics. *Reviews of Modern Physics* **82**, 1793–1842.
- Gill AK, Petkov EE, Safronova AS, Kantsyrev VL, Childers RR, Schultz KA, Shlyaptseva VV, Shrestha IK and Cooper MC (2017) No Title. *2017 Annual Meeting of the Far West Section*, Merced, California, USA. No. E3.13
- Griem H.R. (2005). *Principles of Plasma Spectroscopy*. Cambridge: Cambridge Univ. Press.
- Gu MF (2008) The flexible atomic code. *Canadian Journal of Physics* **86**, 675–689.
- Hagena OF (1972) Cluster formation in expanding supersonic jets: effect of pressure, temperature, nozzle size, and test gas. *The Journal of Chemical Physics* **56**, 1793.
- Hayashi Y, Fukuda Y, Faenov AY, Kando M, Kawase K, Pikuz TA, Homma T, Daido H and Bulanov SV (2010) Intense and reproducible K $\alpha$  emissions from micron-sized Kr cluster target irradiated with intense femtosecond laser pulses. *Japanese Journal of Applied Physics* **49**, 126401.
- Honda H, Miura E, Katsura K, Takahashi E and Kondo K (2000) Evidence for wavelength dependence of Xe M-shell emission from clusters. *Physical Review A* **61**, 023201.
- Jha J and Krishnamurthy M (2008) Hotter electron generation in doped clusters. *Journal of Physics B: Atomic, Molecular and Optical Physics* **41**, 41002.
- Kantsyrev VL, Schultz KA, Shlyaptseva VV, Petrov GM, Safronova AS, Petkov EE, Shrestha I, Cline W, Wiewior P and Chalyy O (2016a) Influence of Xe and Kr impurities on x-ray yield from debris-free plasma x-ray sources with an Ar supersonic gas jet irradiated by femtosecond near-infrared-wavelength laser pulses. *Physical Review E* **94**, 053203.
- Kantsyrev VL, Schultz KA, Shlyaptseva VV, Safronova AS, Cooper MC, Shrestha IK, Petkov EE, Stafford A, Moschella JJ, Schmidt-Petersen MT, Butcher CJ, Kemp GE, Andrews SD and Fournier KB (2016b) Study of laser-generated debris free x-ray sources produced in a high-density linear Ar, Kr, Xe, Kr/Ar and Xe/Kr/Ar mixtures gas jets by 2w, sub-ps LLNL Titan laser. *Bulletin of the American Physical Society* **61**, 411.
- Kantsyrev VL, Schultz KA, Shlyaptseva VV, Safronova AS, Shrestha IK, Petrov GM, Moschella JJ, Petkov EE, Stafford A, Cooper MC, Weller ME, Cline W, Wiewior P and Chalyy O (2016c) Study of x-rays produced from debris-free sources with Ar, Kr and Kr/Ar mixture linear gas jets irradiated by UNR Leopard laser beam with fs and ns pulse duration. *High Energy Density Physics* **19**, 11–22.
- Kemp GE, Link A, Ping Y, McLean HS, Patel PK, Freeman RR, Schumacher DW, Tiedje HF, Tsui YY, Ramis R and Fedosejevs R (2015) On specular reflectivity measurements in high and low-contrast relativistic laser-plasma interactions. *Physics of Plasmas* **22**, 013110.
- Kim KY, Milchberg HM, Faenov AY, Magunov AI, Pikuz TA and Skobelev IY (2006) X-ray spectroscopy of 1 cm plasma channels produced by self-guided pulse propagation in elongated cluster jets. *Physical Review E – Statistical, Nonlinear, and Soft Matter Physics* **73**, 066403.
- Kondo K, Borisov AB, Jordan C, Mc Pherson A, Schroeder WA, Boyer K and Rhodes CK (1997) Wavelength dependence of multiphoton-induced Xe (M) and Xe (L) emissions from Xe clusters. *Journal of Physics B: Atomic, Molecular and Optical Physics* **30**, 2707–2716.
- Kugland NL, Neumayer P, Döppner T, Chung H-K, Constantin CG, Girard F, Glenzer SH, Kemp A and Niemann C (2008) High contrast Kr gas jet K alpha x-ray source for high energy density physics experiments. *The Review of Scientific Instruments* **79**, 10E917.
- Lamour E, Prigent C, Rozet JP and Vernhet D (2007) X-ray production in short laser pulse interaction with rare gas clusters. *Journal of Physics: Conference Series* **88**, 12035.
- Last I, Schek I and Jortner J (1997) Energetics and dynamics of Coulomb explosion of highly charged clusters. *The Journal of Chemical Physics* **107**, 6685.

- Maddox BR, Park HS, Remington BA, Izumi N, Chen S, Chen C, Kimminau G, Ali Z, Haugh MJ and Ma Q (2011) High-energy x-ray backlighter spectrum measurements using calibrated image plates. *Review of Scientific Instruments* **82**, 023111.
- Malka V, Faure J, Marquès JR, Amiranoff F, Rousseau P, Ranc S, Chambaretz JP, Najmudin Z, Walton B, Mora P, Solodov A and Amiranoff F (2001) Characterization of electron beams produced by ultra-short (30 fs) laser pulses. *Physics of Plasmas* **8**, 2605–2608.
- Müller M, Kühl F-C, Großmann P, Vrba P and Mann K (2013) Emission properties of ns and ps laser-induced soft x-ray sources using pulsed gas jets. *Optics Express* **21**, 12831–12842.
- Namba S, Hasegawa N, Nagashima K, Kawachi T, Kishimoto M, Sukegawa K and Takiyama K (2006) Efficient electron heating in nitrogen clusters irradiated with intense femtosecond laser pulses. *Physical Review A* **73**, 013205.
- Parra E, Alexeev I, Fan J, Kim KY, McNaught SJ and Milchberg HM (2001) X-ray and extreme ultraviolet emission induced by variable laser pulse-width irradiation of Ar and Kr clusters and droplets. *Technical Digest. Summaries of papers presented at the Conference on Lasers and Electro-Optics. Postconference Technical Digest (IEEE Cat. No.01CH37170)* **62**, 5931–5934.
- Petrov GM, Davis J, Velikovich AL, Kepple P, Dasgupta A and Clark RW (2005) Dynamics of a Xe cluster plasma produced by an intense ultrashort pulse KrF laser. *Physics of Plasmas* **12**, 063103.
- Prigent C, Deiss C, Lamour E, Rozet J-P, Vernhet D and Burgdörfer J (2008) Effect of pulse duration on the x-ray emission from Ar clusters in intense laser fields. *Physical Review A* **78**, 053201.
- Schroeder WA, Nelson TR, Borisov AB, Longworth JW, Boyer K and Rhodes CK (2001) An efficient, selective collisional ejection mechanism for inner-shell population inversion in laser-driven plasmas. *Journal of Physics B: Atomic, Molecular and Optical Physics* **34**, 297–319.
- Schroeder WA, Omenetto FG, Borisov AB, Longworth JW, McPherson A, Jordan C, Boyer K, Kondo K and Rhodes CK (1998) Pump laser wavelength-dependent control of the efficiency of kilovolt x-ray emission from atomic clusters. *Journal of Physics B* **31**, 5031–5051.
- Schultz KA (2017) *The Experimental Study of Characterized Noble Gas Puffs Irradiated by Ultra-Short Laser Pulses Compared with X-Pinches as an X-Ray Source* (Ph.D. Dissertation). University of Nevada, Reno.
- Schultz KA, Kantsyrev VL, Safronova AS, Moschella JJ, Wiewior P, Shlyapteva VV and Weller ME (2016) Characterization of pure and mixed Ar, Kr and Xe gas jets generated by different nozzles and a study of X-ray radiation yields after interaction with a sub-ps laser pulse. *Physics of Plasmas* **23**, 101207.
- Sharma P and Vatsa RK (2009) Generation of multiply charged atomic ions of halogens using second harmonic of nanosecond Nd:YAG laser. *Current Applied Physics* **9**, 140–143.
- Shim B, Hays G, Zgadzaj R, Ditmire T and Downer MC (2007) Enhanced harmonic generation from expanding clusters. *Physical Review Letters* **98**, 98–101.
- Wachulak PW, Wegrzynski L, Zapraany Z, Bartnik A, Fok T, Jarocki R, Kostecki J, Szczurek M, Korytar D and Fiedorowicz H (2014) Extreme ultraviolet tomography of multi-jet gas puff target for high-order harmonic generation. *Applied Physics B: Lasers and Optics* **117**, 253–263.
- Zhang L, Chen L-M, Yuan D-W, Yan W-C, Wang Z-H, Liu C, Shen Z-W, Faenov A, Pikuz T, Skobelev I, Gasilov V, Boldarev A, Mao J-Y, Li Y-T, Dong Q-L, Lu X, Ma J-L, Wang W-M, Sheng Z-M and Zhang J (2011) Enhanced K $\alpha$  output of Ar and Kr using size optimized cluster target irradiated by high-contrast laser pulses. *Optics Express* **19**, 25812.
- Zhvaniya IA, Dzhidzhoev MS and Gordienko VM (2017) Femtosecond laser excitation of mixed Ar/Kr clusters: peculiarities of K-line x-ray production from nanoplasma under varied fraction of initial gas components. *Laser Physics Letters* **14**, 96001.